J. Ocean Univ. China (Oceanic and Coastal Sea Research)
https://doi.org/10.1007/s11802-022-4847-z
ISSN 1672-5182, 2022 21 (1): 113-123
http://www.ouc.edu.cn/xbywb/
E-mail:xbywb@ouc.edu.cn

Effect of Carbonation and Drying-Wetting Cycles on Chloride Diffusion Behavior of Coral Aggregate Seawater Concrete

DA Bo[1), 3), 4)], LI Yipeng[1)], YU Hongfa[2), *], MA Haiyan[2), *], CHEN Haoyu[5)], DOU Xuemei[2)], and WU Zhangyu[2)]

1) *College of Harbour, Coastal and Offshore Engineering, Hohai University, Nanjing* 210098, *China*
2) *Department of Civil and Airport Engineering, Nanjing University of Aeronautics and Astronautics, Nanjing* 210016, *China*
3) *Key Laboratory of Coastal Disaster and Defence of Ministry of Education, Hohai University, Nanjing* 210098, *China*
4) *Nantong Institute of Marine and Offshore Engineering, Hohai University, Nantong* 226300, *China*
5) *CCCC Infrastructure Maintenance Group Company Limited, Beijing* 100010, *China*

(Received November 23, 2020; revised May 17, 2021; accepted June 9, 2021)

Abstract Based on seawater immersion, drying-wetting cycles, carbonation and drying-wetting cycles for coral aggregate seawater concrete (CASC) with different strength grades, the effect of carbonation and drying-wetting cycles on chloride diffusion behavior of CASC is studied. The results show that the free surface chloride concentration (C_s), free chloride diffusion coefficient (D_f) and time-dependent index (m) of CASC in the drying-wetting cycles is obviously higher than that in seawater immersion. The D_f and m of CASC of carbonation and drying-wetting cycles is higher than that in the drying-wetting cycles. Carbonation increases the D_f and m of CASC, which is against CASC to resist chloride corrosion. The corrosion possibility of CASC structures in different exposed areas is as follows: splash zone (carbonation and drying-wetting cycles) > tidal zone (drying-wetting cycles) > underwater zone (seawater immersion). Besides, the chloride diffusion rate of C65-CASC is 17.8%–63.4% higher than that of C65-ordinary aggregate concrete (OAC) in seawater immersion (underwater zone). Therefore, anti-corrosion measures should be adopted to improve the service life of CASC structure in the oceanic environment.

Key words coral aggregate seawater concrete; chloride diffusion; seawater immersion; drying-wetting cycles; carbonation and drying-wetting cycles

1 Introduction

Islands in the South China Sea are far away from the mainland, and there are no sandstones and freshwater. The application of coral aggregate seawater concrete (CASC) using coral, coral sand and seawater as primary raw materials is of great significance for the ocean engineering (Yu *et al*., 2017; Yang *et al*., 2018; Lyu *et al*., 2019; Ma *et al*., 2019, 2020). However, chloride corrosion, drying-wetting cycles and carbonation will significantly affect the concrete durability in the oceanic environment (Chen *et al*., 2008; Da *et al*., 2018; Liu *et al*., 2018; Wu *et al*., 2020). Therefore, studies on chloride diffusion behavior of CASC in the carbonation and drying-wetting cycles is of great importance on civil engineering.

Da *et al*. (2016a, 2020) find that coral aggregates are a kind of naturally porous structural materials. CASC has chloride diffusion characteristics of high initial free chloride concentration (C_0), high free surface chloride concentration (C_s) and high apparent chloride diffusion coefficients (D_a), and its C_0 (0.11%–0.21%) is much higher than the chloride threshold concentration (C_{cr}) of common steel (about 0.05%), which leads to extremely severe corrosion, affecting the safety and durability of CASC structures. Real *et al*. (2018) studied on chloride diffusion behavior of lightweight aggregate concrete (LAC), and find that the chloride penetration at a certain depth were higher in LAC with lightweight aggregates of higher porosity. Bogas *et al*. (2019) found that when the same strength grade, the LAC can have similar better carbonation resistance performance than ordinary aggregate concrete (OAC) in the laboratory or oceanic environments. In the research of chloride diffusion behavior of OAC, Meijers *et al*. (2005) found that in the drying-wetting cycles, corrosion products continuously are produced in OAC, which leads to its destruction. Besides, the degradation rate of OAC in the drying-wetting cycles is much faster

* Corresponding authors. E-mail: yuhongfa@nuaa.edu.cn
E-mail: mahaiyan@nuaa.edu.cn

than that in seawater immersion. Yu *et al*. (2019) found that in the drying process, chloride salt enters the concrete due to the evaporation of H_2O, resulting in crystallization pressure, destroys the crystallization zone of concrete. Therefore, the drying-wetting cycles accelerate the speed of chloride penetrating OAC. Jin *et al*. (2007) found that carbonation can increase the chloride concentration in OAC. The free chloride diffusion coefficient (D_f) increase, and the growth rate of D_f increases with the extension of exposure time (t). Zhang *et al*. (2011, 2017) study on chloride diffusion properties in low-density (LD) and high-density (HD) calcium-silicate-hydrate, and a numerical method of directly achieving diffusivities is proposed. At present, researches on chloride diffusion behavior of concrete mainly focus on OAC and LAC. Therefore, for the highly porous characteristics of CASC and the real oceanic environment characteristics, this paper studies how carbonation and drying-wetting cycles influence chloride diffusion of CASC.

With the method of natural diffusion, the free chloride concentration (C_f), total chloride concentration (C_t) of CASC in seawater immersion, drying-wetting cycles and carbonation and drying-wetting cycles are systematically tested. The rule of chloride concentration is worked out. The chloride binding capacity (R), C_s, D_f and time-dependent index (m) of CASC with different strength are studied, compared with the durability parameters of OAC. The rule of chloride diffusion of CASC in the carbonation and drying-wetting cycles is summarized, which provides theoretical basis for the application of CASC in the ocean engineering.

2 Experiments

2.1 Raw Materials

The coral sands are from an island in the South China Sea, chloride concentration is 0.112%, apparent density is 2500 kg m^{-3}, bulk density is 1115 kg m^{-3}, porosity is 45.0% and fineness modulus is 2.9. The coral (Da *et al*., 2016b) is also from an island in the South China Sea, chloride concentration is 0.074%, apparent density is 2300 kg m^{-3}, bulk density is 1000 kg m^{-3}, porosity is 58.5%, cylinder compressive strength is 3.8 MPa, and the cylinder compress strength is tested according to Lightweight aggregates and its test methods Part 1: Test methods for lightweight aggregates (GB/T 17431.2-2010). Ordinary Portland cement P·II 52.5, Class I fly ash (FA), S95 grinding slag (SG) and JM-B naphthalene water-reducer are chosen. Seawater is prepared according to ASTM D1141-2003, in which the mass ratio of NaCl: Na_2SO_4:$MgCl_2$·$6H_2O$:KCl:$CaCl_2$ = 24.5:4.1:11.1:0.7:1.2 Yu *et al*. (2019).

2.2 Experiment Scheme

Table 1 shows the mix proportion of CASC. Among them, W/B is the water-binder ratio. The test method according to Standard for test methods of long-term performance and durability of ordinary concrete (GB/T 50082-2009). The size of the sample is 100 mm × 100 mm × 100 mm, the curing age is 28 d, the curing temperature is (20 ± 3)℃, the relative humidity is (70 ± 10)%, and the CO_2 concentration is (20 ± 3)%. Variables include seawater immersion (P, simulates the underwater zone), drying-wetting cycles (PG, simulates the tidal zone) and drying-wetting-carbonation cycles (PT, simulates the splash zone). The exposure time of P is 0, 30, 78 and 120 d respectively. The cycle times of PG and PT are 2, 4, 6, 8, 10, 12 and 14 respectively, and one cycle lasts 6 d. The cycle system of PG is immersion (2 d) → drying (2 d) → air-drying (2 d). The cycle system of PT is immersion (2 d) → drying (2 d) → carbonation (2 d). Fig.1 shows the schematic diagram of cycle system.

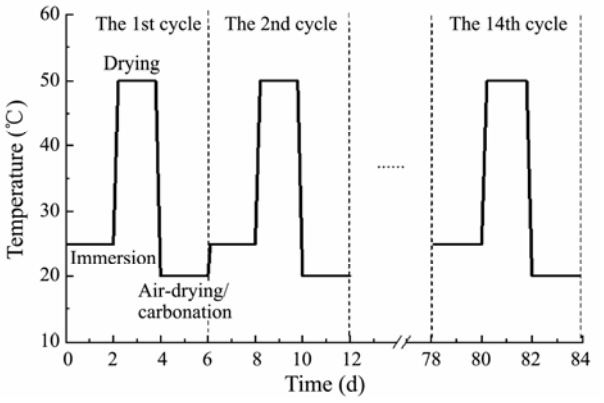

Fig.1 Schematic diagram of cycle system.

Table 1 Mix proportion of CASC

Concrete strength	Cement (kg)	SG (kg)	FA (kg)	Coral sand (kg)	Coral (kg)	Seawater (kg)	Water-reducer (kg)	W/B	Slump (mm)	28 d f_{cu}	Density (kg m^{-3})
C30	275	150	75	873	582	296	8.3	0.59	125	57.4	2167
C50	620	120	60	860	369	221	6.0	0.28	120	64.9	2183
C55	780	150	70	700	300	250	6.0	0.20	255	68.9	2267

2.3 Tests and Analysis Method

2.3.1 Powder collection

Collect powder from CASC samples at different t. Drilling depth is 0–5, 5–10, 10–15, 15–20, 20–25, 25–30, 30–35, 35–40, 40–45 and 45–50 mm. Fig.2 is drilling locations of CASC powder.

2.3.2 Chloride concentration and chloride binding capacity

According to Testing code of concrete for port and waterwog engineering (JTJ 270-1998), the C_f and C_t are tested by water-soluble and acid-soluble method respectively. Besides, according to the R defined by Tang

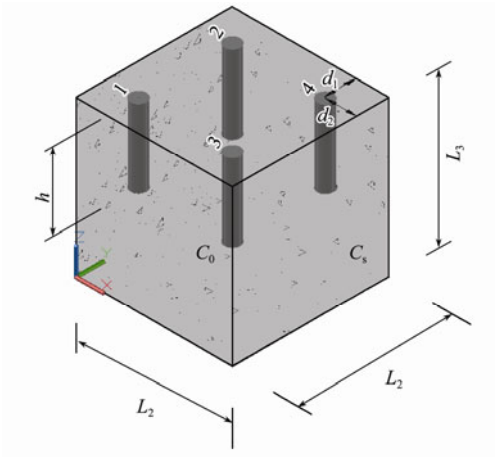

Fig.2 Drilling locations of CASC powder. Note: 1, 2, 3 and 4 in the figure are powder collection points. The minimum vertical distance between the collection points and the two sides is $d_1=d_2=20$ mm respectively. Drilling depth is h.

et al. (2008), and the relationship between C_f and C_t of concrete structures, R is expressed as follows:

$$\begin{cases} C_b = C_t - C_f \\ R = \dfrac{\partial C_b}{\partial C_f} = \dfrac{\partial (C_t - C_f)}{\partial C_f} = \dfrac{\partial C_t}{\partial C_f} - 1 = K - 1, \\ C_t = KC_f \end{cases} \quad (1)$$

where C_t is the total chloride concentration (%); C_f is the free chloride concentration (%), when t = 0 day, C_f = initial chloride concentration (C_0); C_b is the binding chloride concentration (%); R is the chloride binding capacity. The R of concrete will not only reduce C_s, but also reduce C_f. When C_f is lower than C_{cr}, steel bars will not rust.

2.3.3 Free surface chloride concentration and free chloride diffusion coefficient

The C_f at an average depth of 2.5, 7.5, 12.5, 17.5, 22.5, 27.5, 32.5, 37.5, 42.5 and 47.5 mm is measured, and the C_s is obtained according to the chloride diffusion model (Yu *et al*., 2002; Da *et al*., 2016c). The three-dimensional chloride diffusion model of concrete as follows:

$$\begin{cases} \dfrac{\partial^2 C_f}{\partial x^2} + \dfrac{\partial^2 C_f}{\partial y^2} + \dfrac{\partial^2 C_f}{\partial z^2} = \dfrac{1}{D}\dfrac{\partial C_f}{\partial t} \\ \text{Initial condition: } t = 0,\ x > 0,\ y > 0,\ z > 0,\ C_f = C_0 \\ \text{Boundary conditions:} \\ t > 0,\ x = 0,\ C_f = C_s;\ x = L_1,\ C_f = C_s \\ t > 0,\ y = 0,\ C_f = C_s;\ y = L_2,\ C_f = C_s \\ t > 0,\ z = 0,\ C_f = C_s;\ z = L_3,\ C_f = C_s \end{cases} \quad (2)$$

Therefore, the three-dimensional chloride diffusion homogeneous model of concrete is obtained as follows:

$$C_f = C_s + \sum_{m=1,3,5}^{\infty} \sum_{n=1,3,5}^{\infty} \sum_{p=1,3,5}^{\infty} \frac{64}{mnp\pi^3}(C_0 - C_s)\sin\left(\frac{m\pi}{L_1}x\right)\sin\left(\frac{n\pi}{L_2}y\right)\sin\left(\frac{p\pi}{L_3}z\right)\exp\left[-D_a\left(\frac{m^2\pi^2}{L_1^2} + \frac{n^2\pi^2}{L_2^2} + \frac{p^2\pi^2}{L_3^2}\right)t\right], \quad (3)$$

where D_a is the apparent chloride diffusion coefficient; L_1, L_2 and L_3 are the depths in the directions of x, y and z, respectively.

According to Maage *et al*. (1996), the D_f is expressed as follows:

$$D_f = (1+R)D_a . \quad (4)$$

The D_f reflects the chloride penetration rate of concrete. The higher the D_f is, the faster the chloride concentration increases.

2.3.4 Time-dependent index of free chloride diffusion coefficient

Concrete hydration is a slow process. As the hydration goes on, the porous structure of concrete is gradually improved, and its D_f is slowly reduced. Thomas *et al*. (1999) found that the rule of D_f with t is expressed as follows:

$$D_f(t) = A \cdot t^{-m}, \quad (5)$$

where m is the time-dependent index of D_f; A is a fitting parameter.

3 Results and Discussion

3.1 Seawater Immersion

3.1.1 Chloride concentration

Fig.3 shows the chloride concentration of CASC in seawater immersion. Among them, the concrete strength grade is C65, and the t is 0, 30, 78 and 120 d, respectively. It shows that the C_f and C_t of CASC increase with the extension of t and decrease gradually as the depth of diffusion grows, and tend to be stable at a certain depth. Besides, when the depth is 2.5 and 7.5 mm, C_t of C65P under 120 days' exposure increases by 23.2% and 48.5% respectively compared with that under 30 days' exposure. When the depth reaches 12.5 mm, the relative growth rate of C_f remains stable at 4.0%–10.4%. The main reasons are as follows: the chloride concentration increases gradually with the extension of t. However, as CASC hydrates, the internal pores structure of concrete is improved, which makes various ions silt up the pores of CASC, thus blocking the channel through which chloride diffuses, and then enhancing the capacity of against chloride diffusion. Therefore, with the extension of t, the growth rate of chloride concentration in CASC gradually slows down.

3.1.2 Chloride binding capacity

According to the analysis, the R of C50P, C60P and C65P are 0.1967, 0.2466 and 0.1486, respectively (C50P: $y = 1.1967x$, $r^2 = 0.9068$; C60P: $y = 1.2466x$, $r^2 = 0.9385$;

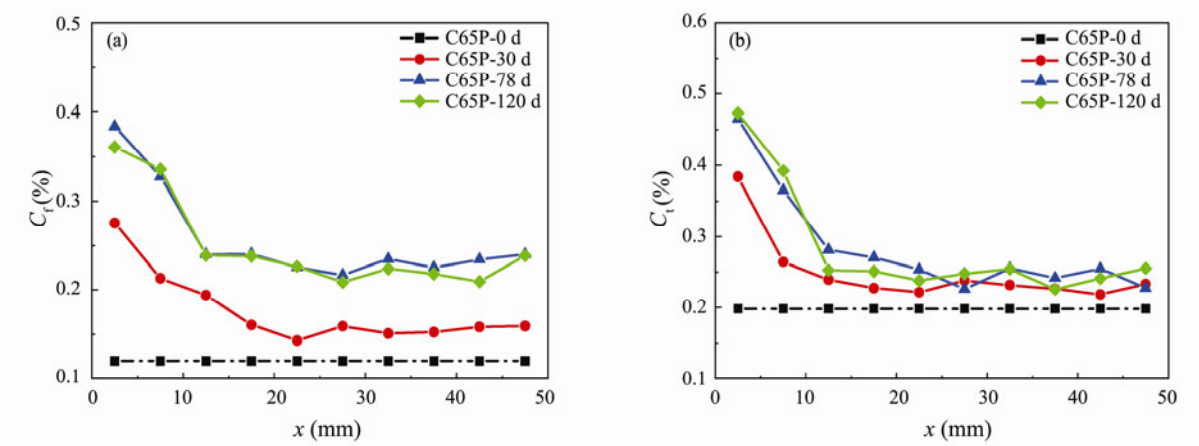

Fig.3 Chloride concentration of CASC in seawater immersion. C50P indicates that the concrete strength is C50 and the cycle system is seawater immersion (P).

C65P: $y=1.1486x$, $r^2=0.8732$). Besides, the growth of C_f is linear with that of C_t, which is not related to t. The main reason is that the concrete absorbing chloride is a comprehensive process of physically and chemically. The t only affects value of C_f and C_t but does not affect absorption. Therefore, there is no need to take into account the effect of t in the study on R of CASC.

3.1.3 Free surface chloride concentration

3.1.3.1 Different exposure time

Table 2 shows the C_s of CASC in seawater immersion. It indicates that the C_s of CASC increases with the extension of t. The growth is faster at first and tends to be stable later. Under the same t, C_s decreases with the increase of concrete strength. In seawater immersion, the relationship between C_s and t accords with the $(1-m)$ power exponent (Table 2). Besides, when exposed for 30, 78 and 120 d, the C_s of C65P decreases by 23.2%, 20.7% and 26.1%, respectively, compared with that of C50P. The main reasons are as follows: for high strength CASC, with the extension of t, its compactness gradually increases due to the continuous hydration, and the internal micro-pore structure improves continuously, blocking the channel through which chloride diffuses, and enhancing the capacity of against chloride diffusion. Therefore, the growth rate of C_s gradually slows down.

Table 2 Relationship between C_s and t of CASC in seawater immersion

No.	Fitting equations	C_0 (%)	k	r
C50P	$C_s = k \cdot t^{1-m} + C_0$	0.176	0.046	0.9799
	$C_s = k \cdot t^{\frac{1-m}{2}} + C_0$		0.123	0.8862
C60P	$C_s = k \cdot t^{1-m} + C_0$	0.169	0.052	0.9776
	$C_s = k \cdot t^{\frac{1-m}{2}} + C_0$		0.117	0.8084
C65P	$C_s = k \cdot t^{1-m} + C_0$	0.153	0.085	0.9565
	$C_s = k \cdot t^{\frac{1-m}{2}} + C_0$		0.139	0.6624

Notes: k is a fitting parameter, r is a correlation coefficient.

3.1.3.2 Different concrete type

Fig.4 shows the C_s of CASC and OAC in seawater immersion. It indicates that when exposed for 30, 78 and 120 d, the C_s of C60P-CASC increases by 31.3%, 59.7% and 14.5% respectively compared with that of C60P-OAC. The main reasons are as follows: CASC is lightweight aggregate concrete (LAC) with large porosity and strong absorbency (Fig.5) (Cheng *et al*., 2017; Wang *et al*., 2020). Its porous structure becomes the channel through which chloride diffuses. Besides, CASC is mixed with seawater, which contains a lot of chlorine salts, the initial free chloride concentration (C_0) of CASC reaches 0.11%–0.21% (Liu *et al*., 2019; Wang *et al*., 2019), resulting in a higher C_s.

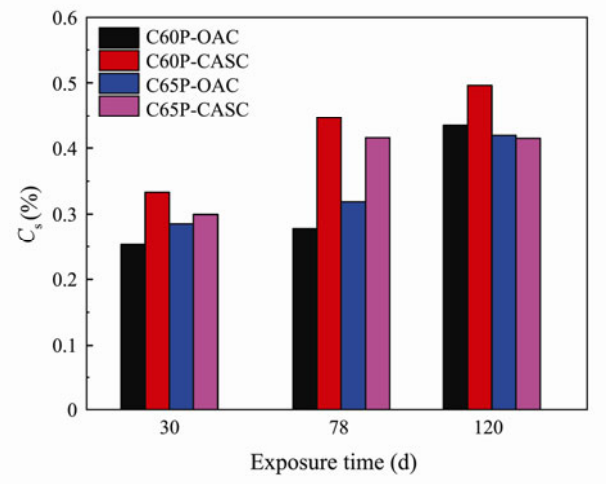

Fig.4 C_s of CASC and OAC in seawater immersion.

3.1.4 Free chloride diffusion coefficient

3.1.4.1 Different exposure time

It is known by analysis the D_f of CASC decreases power exponentially with the extension of exposure time (t) in seawater immersion (C50P: $D_f=9E\text{-}11t^{-0.544}$, $r^2=0.9406$; C60P: $D_f=9E\text{-}11t^{-0.622}$, $r^2=0.9495$; C65P: $D_f=$

2E-10$t^{-0.766}$, r^2=0.8361), and the D_f of CASC decreases gradually with the increase of concrete strength. When exposed for 78 and 120 d, the D_f of C65P decreases by 31.49% and 68.84%, respectively, compared with that under 30 days' exposure. The main reason is as follows: FA and SG are added to CASC. In the early stage, the hydration of cement, FA and SG in CASC are not sufficient, so the filling and pozzolanic effects of FA and SG cannot be fully exerted, which increases the D_f. However, with the extension of t, the C-S-H gel gradually forms in the capillary interstice due to pozzolanic effect, which lowers the porosity and pores size of CASC. Thus, the D_f is decreasing and the capacity of against chloride diffusion of CASC is enhancing.

Fig.5 Porous structure of CASC. (a), coral-1; (b), coral-2; (c), coral-3.

3.1.4.2 Different concrete type

Fig.6 shows the D_f of CASC and OAC in seawater immersion. The results show that the D_f of CASC and OAC decreases gradually with the extension of t, and the D_f of CASC is much higher than that of OAC at the same t. When exposed for 30, 78 and 120 d, the D_f of C65P-CASC is 28%, 63.4% and 17.8% higher than that of C65P-OAC respectively. The m of C60P-OAC (0.940) and C65P-OAC (0.980) is higher than that of C60P-CASC (0.618) and C65P-CASC (0.767), indicating that the decline rate of D_f of OAC is faster than that of CASC. This is mainly due to the porous structure of coral aggregate, which makes it easier for chloride in seawater or sea wind to enter CASC.

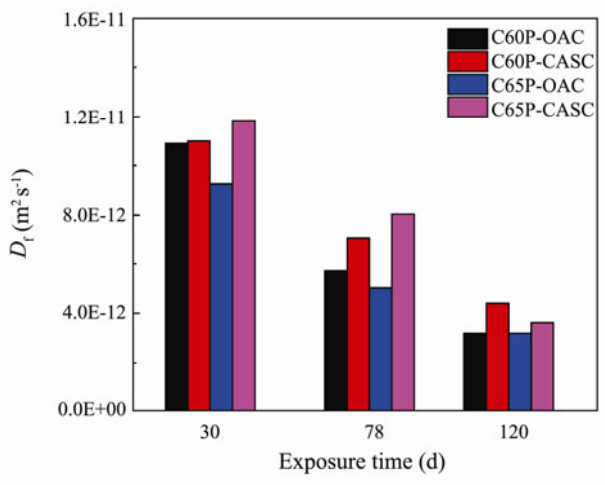

Fig.6 D_f of CASC and OAC in seawater immersion.

3.2 Drying-Wetting Cycles

3.2.1 Chloride concentration

3.2.1.1 Different cycle times

Fig.7 shows the chloride concentration of CASC in the drying-wetting cycles. Among them, the concrete strength grade is C65, and the cycle times is 2, 4, 6, 8, 10, 12 and 14, respectively. It indicates that: at the same diffusion depth, the C_f and C_t of CASC increase with the increase of cycle times. Besides, when the diffusion depth is 7.5 mm, the C_f of C65PG increases by 25%, 31%, 77%, 71%, 50% and 66% respectively at 4th, 6th, 8th, 10th, 12th and 14th cycles compared with that at 2nd cycles. When the diffusion depth is 37.5 mm, the C_f of C65PG increases by 0.7%, 4.5%, 22.8%, 32.0% and 22.0%, respectively, at 6th, 8th, 10th, 12th and 14th cycles compared with that at 2nd cycles. The main reason is that when the concrete is water-saturated, chloride begins to permeate into the concrete because of diffusion. When the external environment is dry, the H_2O in the concrete evaporates outward gradually. The whole process is accompanied by water draining outward and chloride diffusing inward. At a certain depth of concrete, the chloride concentration will increase, and the concentration difference of chloride will increase. After many cycles, the chloride concentration reaches its peak in a certain depth. From this peak inward, chloride mainly is transferred by diffusion. From this peak outward, chloride is mainly transferred by capillary absorption and moisture evaporation. With the increase of cycle times, the peak point of chloride concentration tends to move to the interior of concrete. The chloride accumulation and transmission rate mainly depend on the drying-wetting cycle times. Therefore, the more the cycles, the faster the peak point of chloride concentration moves inward.

3.2.1.2 Different cycle system

Fig.8 shows the chloride concentration of CASC in seawater immersion and drying-wetting cycles. Among then, the concrete strength grade is C50, and the t is 120 days'. It indicates that there is little difference between the C_f of C50P and that of C50PG at the concrete surface, while the difference of C_t between C50P and C50PG is

17.5% at the concrete surface. With the increase of diffusion depth, the difference of C_f between C50P and C50PG increases gradually. When the diffusion depth is 12.5, 17.5 and 22.5 mm, the C_f (C_t) of C50PG increases by 32% (48%), 54% (52%) and 61% (50%), respectively, compared with that of C50P. When the diffusion depth reaches 27.5 mm, the difference of C_f between C50P and C50PG tends to be stable. The results show that the drying-wetting cycles can promote the chloride diffusion of CASC, and barely affect the surface of concrete, but it significantly influences the chloride concentration as the depth increases.

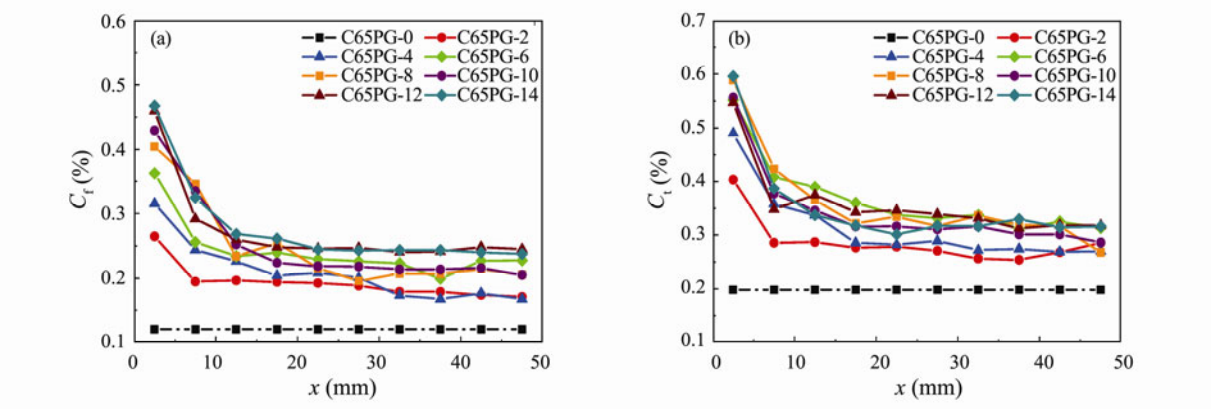

Fig.7 Chloride concentration of CASC in the drying-wetting cycles. (a), C_f; (b), C_t.

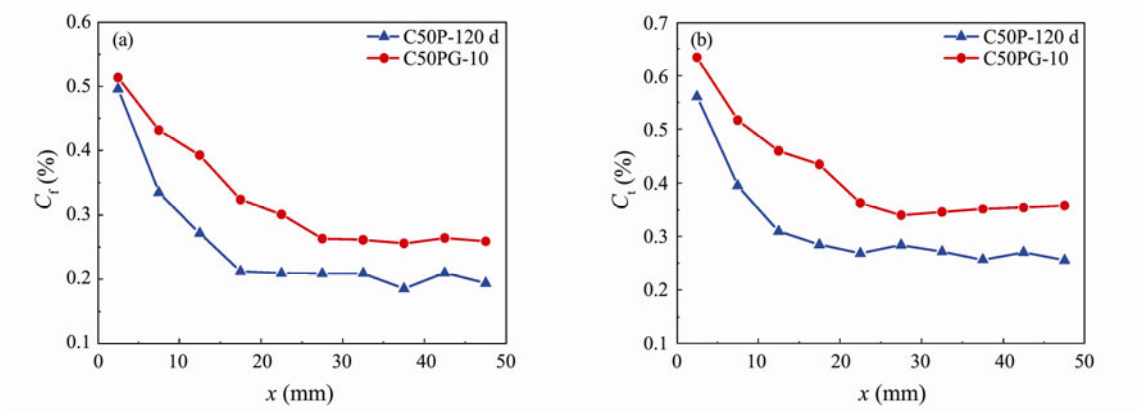

Fig.8 Chloride concentration of CASC in seawater immersion and drying-wetting cycles. (a), C_f; (b), C_t.

3.2.2 Chloride binding capacity

According to the analysis, there is a linear relationship between C_f and C_t of C50PG in the drying-wetting cycles (C50PG-2: $y=1.4193x$, $r^2=0.9063$; C50PG-4: $y=1.3679x$, $r^2=0.9400$; C50PG-6: $y=1.3339x$, $r^2=0.9281$), which is consistent with seawater immersion. Besides, with the increase of drying-wetting cycle times, the R of CASC decreases gradually, and its durability decreases.

3.2.3 Free surface chloride concentration

3.2.3.1 Different cycle times

Table 3 shows the C_s of CASC in the drying-wetting cycles. The results show that the C_s of CASC increases with the increase of cycle times, and the growth is faster at first and tends to be stable later. After 8th cycles, the C_s of CASC almost reaches a steady state. In the drying-wetting cycles, the relationship between C_s and cycle time accords with the $(1-m)$ power exponent (Table 3). Besides, under the same cycle time, C_s decreases with the increase of CASC strength. When the cycle times is 4, 8, 12 and 14, the C_s of C65PG decreases by 16.7%, 13.2%, 10.3% and 10.7%, respectively, compared with that of C50PG. The main reason is as follows: the C_s of CASC mainly depends on the capillary adsorption (concrete surface) of chloride. Concrete absorbs seawater until it is saturated by capillary adsorption. If the external environment becomes dry, the H_2O in the pores will move to the concrete surface, and evaporates through the capillary end. Because only H_2O is evaporated, the chloride concentra-

Table 3 Relationship between C_s and t of CASC in the drying-wetting cycles

No.	Fitting equations	C_0 (%)	k	r
C50P	$C_s = k \cdot t^{1-m} + C_0$	0.176	0.053	0.9831
	$C_s = k \cdot t^{\frac{1-m}{2}} + C_0$		0.136	0.8893
C60P	$C_s = k \cdot t^{1-m} + C_0$	0.169	0.079	0.9496
	$C_s = k \cdot t^{\frac{1-m}{2}} + C_0$		0.148	0.7803
C65P	$C_s = k \cdot t^{1-m} + C_0$	0.153	0.098	0.9067
	$C_s = k \cdot t^{\frac{1-m}{2}} + C_0$		0.168	0.7230

Notes: k is a fitting parameter, r is a correlation coefficient.

tion in the concrete surface is increased, which is much higher than that of the concrete interior. Thus a concentration difference is formed, which drives the chloride in the concrete surface to diffuse to concrete interior. With the increase of concrete strength, the compactness of CASC gradually increases, which enhances the capacity of against chloride diffusion, and slows down the growth rate of C_s.

3.2.3.2 Different cycle system

Fig.9 shows the C_s of CASC in different cycle systems. The results show that when exposed for 30, 78 and 120 days, the C_s of C50PG increases by 8.0%, 1.9% and 2.7% compared with that of C50P, the C_s of C65PG increases by 16.3%, 4.7% and 14.7% compared with that of C65P. That is to say, the C_s of CASC in the drying-wetting cycles is higher than that in seawater immersion, indicating that it is easier for chloride to diffuse into CASC in the drying-wetting cycles than in seawater immersion.

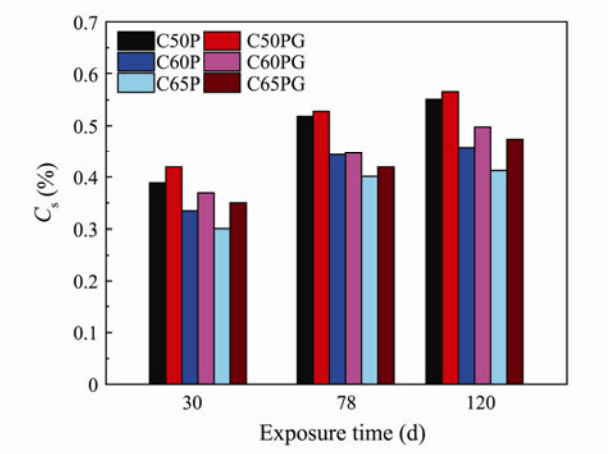

Fig.9 C_s of CASC in seawater immersion and drying-wetting cycles.

3.2.4 Free chloride diffusion coefficient

3.2.4.1 Different cycle times

It is known by analysis the D_f of CASC decreases power exponentially with the increase of cycle times (n) in seawater immersion and drying-wetting cycles (C50PG: D_f=4E-11$n^{-0.690}$, r^2=0.9772; C60PG: D_f=3E-11$n^{-0.857}$, r^2=0.8991; C65PG: D_f=4E-11$n^{-0.907}$, r^2=0.9594), and the D_f of CASC decreases gradually with the increase of concrete strength. The D_f of C50PG is 32%, 25%, 88% and 66% higher than that of C65PG at 4th, 8th, 12th and 14th cycles. The main reasons are as follows: as the hydration goes on, the C-S-H gel gradually forms in the capillary interstice, which reduces the porosity and the size of pores of CASC, thereby decreasing the D_f of CASC. In addition, the higher the strength of CASC is, the denser the structure and the lower the porosity will be, thus reducing the D_f.

3.2.4.2 Different cycle systems

Fig.10 shows the D_f of CASC in seawater immersion and drying-wetting cycles. The results show that when exposed for 30, 78 and 120 d, the D_f of C50PG increases by 20.4%, 20.5% and 33.4%, respectively, compared with that of C50P. The main reasons are as follows: in the drying-wetting cycles, the H_2O in the pores on the CASC surface evaporates rapidly, leaving the salt to crystallize instantly and produce crystallization pressure, which causes the surface to crack. These micro-cracks form the channel for seawater to infiltrate into CASC. When CASC is immersed in seawater again, there is a great difference in chloride concentration between the surface and interior, which accelerates the speed of chloride permeation under capillary adsorption. Therefore, the drying-wetting cycles increase the D_f of CASC and make it easier for chloride to enter CASC, which reduces its durability.

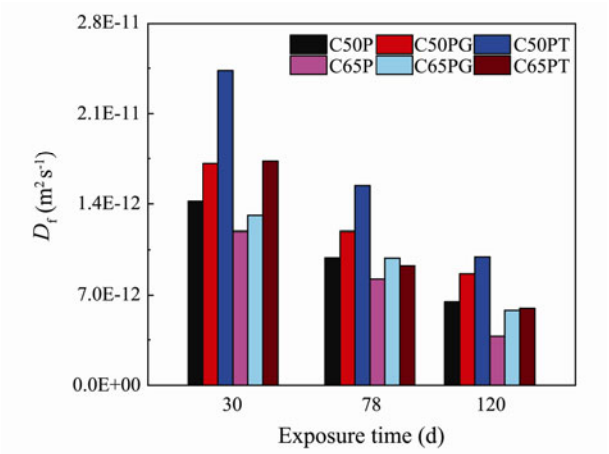

Fig.10 D_f of CASC in the different cycle systems.

3.3 Drying-Wetting-Carbonation Cycles

3.3.1 Chloride concentration

3.3.1.1 Different cycle times

Fig.11 shows the chloride concentration of CASC in the carbonation and drying-wetting cycles. Among them, the cycle time is 2, 4, 6, 8, 10, 12 and 14 respectively. It indicates that: at the same diffusion depth, the C_f of CASC increases with the increase of cycle times. Besides, in the 14th cycle, the chloride concentration of C65PT tends to be steady when the diffusion depth is 11 mm, while the chloride concentration of C50PT is not stable when the diffusion depth is 19 mm. The main reason is that the water saturation of concrete has a significant influence on chloride diffusion, and its water saturation is not only related to the environment humidity, but also related to the compactness of concrete. When CASC changes from saturation to unsaturation, moisture in CASC of high strength penetrates slowly because of its high compactness. However, moisture in CASC of low strength evaporates quickly because of its weak compactness. Before CASC is immersed next time, the transfer of chloride will be hindered by diffusion and capillary absorption, therefore, the transfer will be accelerated, increasing the chloride concentration in CASC. Thus, increasing the strength of CASC can significantly enhance the capacity of against chloride diffusion.

Fig.12 is the surface state of CASC in the carbonation and drying-wetting cycles. It shows that after 14th cycles, the surface state of CASC does not change obviously, and there is no obvious damage on the surface. In addition, Fig.12(c) shows that the carbonation depth of CASC is measured by phenolphthalein reagent. It shows that only C50 is carbonized but C65 is not. After 14th cycles, the carbonation depth of C50 CASC reaches 6.12 mm.

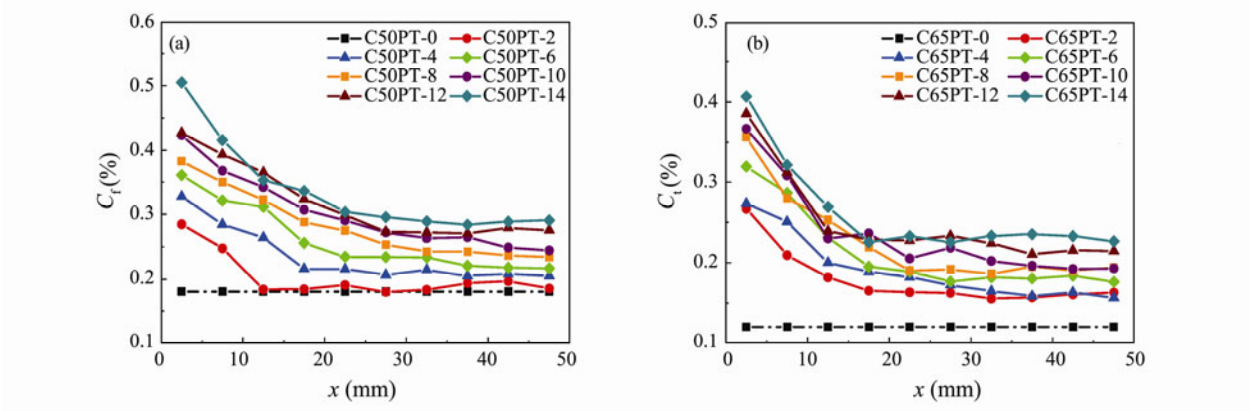

Fig.11 Chloride concentration of CASC in the carbonation and drying-wetting cycles. (a), C50PT; (b), C65PT.

Fig.12 Surface state of CASC in the carbonation and drying-wetting cycles. (a), C50PT-14; (b), C65PT-14; (c), carbonation depth.

3.3.1.2 Different cycle systems

Fig.13 shows the chloride concentration of CASC in the different cycle systems. It indicates that for CASC of high strength (C65P) in seawater immersion, the distribution curve of chloride concentration is relatively smooth, without apparent fluctuation, and monotonous decline. As the strength of CASC decreases, carbonation increases the chloride concentration of CASC, and there obviously exists the 'intersection point' in the distribution curve of chloride concentration of CASC in seawater immersion, carbonation and drying-wetting cycles. The Fig.13(a) shows that: When the diffusion depth < 6 mm, the C_f of CASC is higher in seawater immersion. When the diffusion depth > 6 mm, the C_f of CASC is higher in the carbonation and drying-wetting cycles. Therefore, carbonation will suppress first and then accelerate the chloride concentration of CASC, indicating that carbonation accelerates the increase of C_f, which is against CASC to resist chloride corrosion.

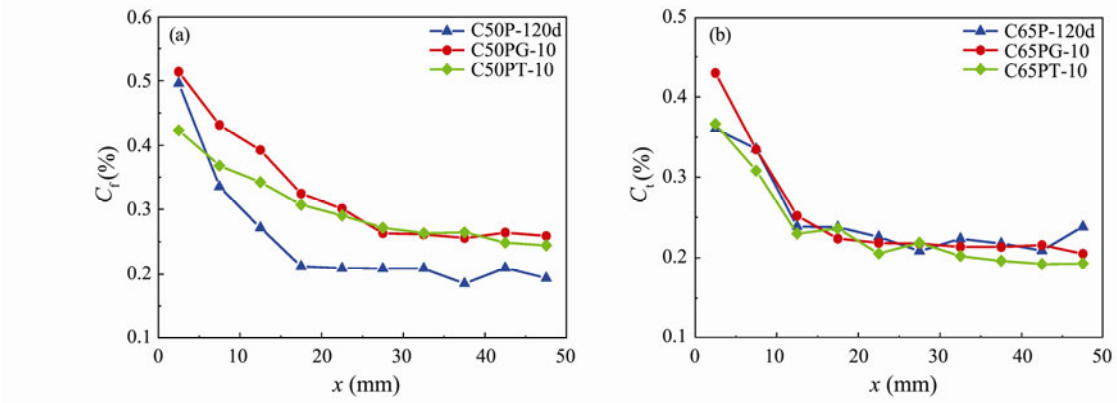

Fig.13 Chloride concentration of CASC in the different cycle systems: (a), C50; (b), C65.

3.3.2 Chloride binding capacity

According to the analysis, there is a linear relationship between C_f and C_t of C50PT in the carbonation and drying-wetting cycles (C50PT-2: $y=1.2998x$, $r^2=0.8005$; C50PT-4: $y=1.2520x$, $r^2=0.9590$; C50PT-6: $y=1.2179x$,

$r^2 = 0.9665$). Besides, as the number of cycles increase, the R of CASC decreases gradually, and its durability weakens.

3.3.3 Free surface chloride concentration

3.3.3.1 Different cycle times

Table 4 shows the C_s of CASC in the carbonation and drying-wetting cycles. It indicates that the C_s of CASC increases with the increase of cycle times. The growth is faster at first and slows down and tends to be stable later. In the carbonation and drying-wetting cycles, the relationship between C_s and cycle time accords with the (1-m) power exponent (Table 4). Besides, under the same cycle time, C_s decreases with the increase of CASC strength. The main reason is that the conversion of $Ca(OH)_2$ to $CaCO_3$ during carbonation enhances the compactness of concrete, which means that carbonation hinders the chloride diffusion. Meanwhile, the number of capillary holes in concrete increases, accelerating the chloride diffusion in concrete, which indicates that carbonation either can promote or hinder the chloride diffusion in concrete. However, the C_s of CASC increases with the extension of carbonation time, and carbonation promotes the chloride diffusion of CASC.

Table 4 Relationship between C_s and t of CASC in the carbonation and drying-wetting cycles

No.	Fitting equations	C_0 (%)	k	r
C50P	$C_s = k \cdot t^{1-m} + C_0$	0.176	0.048	0.9356
	$C_s = k \cdot t^{\frac{1-m}{2}} + C_0$		0.105	0.8724
C60P	$C_s = k \cdot t^{1-m} + C_0$	0.169	0.063	0.8632
	$C_s = k \cdot t^{\frac{1-m}{2}} + C_0$		0.120	0.6894
C65P	$C_s = k \cdot t^{1-m} + C_0$	0.153	0.069	0.9264
	$C_s = k \cdot t^{\frac{1-m}{2}} + C_0$		0.127	0.7543

3.3.3.2 Different cycle systems

Fig.14 shows the C_s of CASC in the different cycle systems. The results show that when exposed for 30, 78 and 120 d, the C_s of C50PT decreases by 8.9%, 29.9% and 20.7% respectively compared with that of C50P, and the C_s of C65PT decreases by 0.5%, 15.3% and 1.3% respectively compared with that of C65P. That is to say, the C_s of CASC in the carbonation and drying-wetting cycles is lower than that in seawater immersion. The main reasons are as follows: The longer time CASC is exposed to seawater, the more easily the chloride will penetrate, thus accelerating the growth rate of C_s.

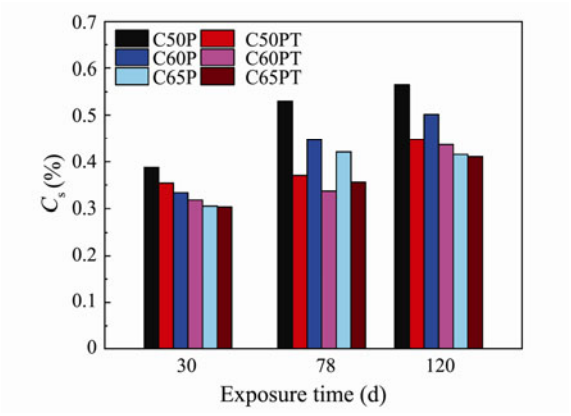

Fig.14 C_s of CASC in the different cycle system.

3.3.4 Free chloride diffusion coefficient

3.3.4.1 Different cycle times

It indicates that the D_f of CASC decreases power exponentially with the increase of cycle times (n) in the carbonation and drying-wetting cycles (C50PT: D_f = 6E-11$n^{-0.767}$, $r^2 = 0.9256$; C60PT: D_f = 5E-11$n^{-0.825}$, r^2 = 0.9777; C65PT: D_f=4E-11$n^{-0.842}$, r^2=0.9492), and the D_f of CASC decreases gradually with the increase of concrete strength. The main reasons are as follows: carbonation results in the micro-structures redistribution of CASC and enlarges the size of micro-pores. Therefore, carbonation speeds up the chloride diffusion and increases the D_f of CASC.

Besides, with the increase of CASC strength, its m increases gradually. The main reason is that with the extension of carbonation time, more $Ca(OH)_2$ is involved in the chemical reaction to produce $CaCO_3$ in concrete, which further enlarges the micro-pores size of CASC. However, the secondary hydration of FA can refine the porous structure of CASC and improve its impermeability. At the same time, the secondary hydration of FA needs to consume some $Ca(OH)_2$. Therefore, when more $Ca(OH)_2$ is converted into $CaCO_3$ in CASC, it will affect the secondary hydration of FA and the refinement of the porous structure, and slow down the decay rate of D_f.

3.3.4.2 Different cycle systems

Fig.15 shows the D_f of CASC in the drying-wetting cycles, carbonation and drying-wetting cycles. The results show that when cycled for 4th, 8th, 12th and 14th times, the D_f of C50PT increases by 41.0%, 64.2%, 18.9% and 1.5%, respectively, compared with that of C50PG, and the D_f of C65PT increases by 31.7%, 19.1%, 33.2% and 19.3%, respectively, compared with that of C65PG,

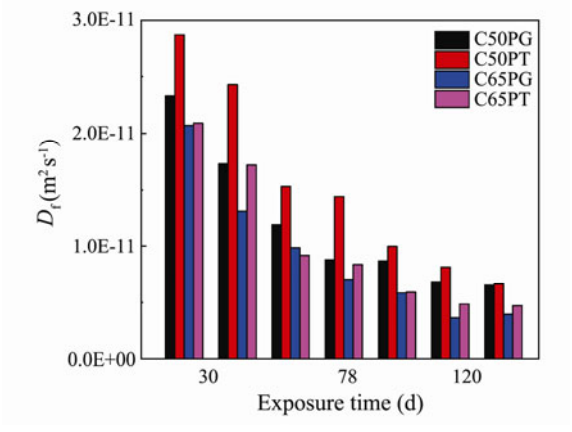

Fig.15 D_f of CASC in the drying-wetting cycles, carbonation and drying-wetting cycles.

indicating that carbonation can significantly increase the D_f of CASC.

4 Conclusions

The C_f and C_t of CASC decrease gradually as chloride diffuses is deeper. When the depth reaches 12.5 mm, the relative growth rate of C_f remains stable at 4.0%−10.4%, and there is a linear relationship between C_f and C_t. Drying-wetting cycles can accelerate the chloride diffusion of CASC and has little effect on the concrete surface, but it significantly influences the chloride concentration as the depth increases. Carbonation accelerates the increase of C_f, which is against CASC to resist chloride diffusion.

The C_s of CASC increases exponentially with the extension of t. The growth rate of C_s of CASC is lower than that of OAC. The D_f of CASC decreases power exponentially with the extension of t. The C_s, D_f of CASC decreases gradually with the increase of concrete strength.

The C_s, D_f and m of CASC in the drying-wetting cycles are obviously higher than that in seawater immersion. The D_f and m of CASC of carbonation and drying-wetting cycles are higher than that in the drying-wetting cycles. It indicates that carbonation and drying-wetting cycles accelerates the chloride diffusion rate but decreases the maximum of chloride concentration. Carbonation increases the D_f and m of CASC.

For the ocean engineering, the corrosion degree of CASC structures in different exposed areas is splash zone (carbonation and drying-wetting cycles) > tidal zone (drying-wetting cycles) > underwater zone (seawater immersion). In addition, the chloride diffusion rate of C65-CASC is 17.8%−63.4% higher than that of C65-OAC in seawater immersion (underwater zone). Therefore, anti-corrosion measures should be adopted to improve the service life of CASC structure in the oceanic environment.

Acknowledgements

The authors gratefully acknowledge the financial supports from the National Natural Science Foundation of China (Nos. 11832013 and 51878350), the Fundamental Research Funds for the Central Universities (No. B2102 02023), the Young Scientific and Technological Talents to Support Project of Jiangsu Association for Science and Technology (No. 027), the Water Conservancy Science and Technology Project of Jiangsu Province (No. 2020 017), the Postdoctoral Research Funding Program of Jiangsu Province (No. 2021K133B), the Ningbo Science and Technology Innovation Project (No. 2020Z040), the Nantong Science and Technology Plan Project (No. JC 2020120), the Open Research Fund of Changjiang River Research Institute of Changjiang Water Resources Committee (No. CKWV2021879/KY).

References

Bogas, J. A., Carrico, A., and Pontes, J., 2019. Influence of cracking on the capillary absorption and carbonation of structural lightweight aggregate concrete. *Cement and Concrete Composites*, **104**: 103382, https://doi.org/10.1016/j.cemconcomp.2019.103382.

Chen, J. K., Jiang, M. Q., and Zhu, J., 2008. Damage evolution in cement mortar due to erosion of sulphate. *Corrosion Science*, **50**: 2478-2483, https://doi.org/10.1016/j.corsci.2008.05.021.

Cheng, S. K., Shui, Z. H., Sun, T., Yu, R., Zhang, G. Z., and Ding, S., 2017. Effects of fly ash, blast furnace slag and metakaolin on mechanical properties and durability of coral sand concrete. *Applied Clay Science*, **141**: 111-117, https://doi.org/10.1016/j.clay.2017.02.026.

Da, B., Yu, H. F., Ma, H. Y., and Wu, Z. Y., 2018. Research on compression behavior of coral aggregate reinforced concrete columns under large eccentric compression loading. *Ocean Engineering*, **155**: 251-260, https://doi.org/10.1016/j.oceaneng.2018.02.037.

Da, B., Yu, H. F., Ma, H. Y., and Wu, Z. Y., 2020. Reinforcement corrosion research based on electrochemical impedance spectroscopy for coral aggregate seawater concrete in a seawater immersion environment. *Journal of Testing and Evaluation*, **48**: 1537-1553, https://doi.org/10.1520/JTE20180197.

Da, B., Yu, H. F., Ma, H. Y., Tan, Y. S., Mi, R. J., and Dou, X. M., 2016a. Chloride diffusion study of coral concrete in a marine environment. *Construction and Building Materials*, **123**: 47-58, https://doi.org/10.1016/j.conbuildmat.2016.06.135.

Da, B., Yu, H. F., Ma, H. Y., Tan, Y. S., Mi, R. J., and Dou, X. M., 2016b. Experimental investigation of whole stress-strain curves of coral concrete. *Construction and Building Materials*, **122**: 81-89, https://doi.org/10.1016/j.conbuildmat.2016.06.064.

Da, B., Yu, H. F., Ma, H. Y., Zhang, Y. D., Zhu, H. W., Yu, Q., *et al*., 2016c. Factors influencing durability of coral concrete structure in South China Sea. *Journal of the Chinese Ceramic Society*, **44**: 254-261, DOI: 10.14062/j.issn.0454-5648.2016.02.11 (in Chinese with English abstract).

Jin, Z. Q., Sun, W., Zhang, Y. S., Jiang, J. Y., and Lai, J. Z., 2007, Interaction between sulfate and chloride solution attack of concretes with and without fly ash. *Cement and Concrete Research*, **37**: 1223-1232, https://doi.org/10.1016/j.cemconres.2007.02.016.

Liu, C., Xie, D. Q., She, W., Liu, Z. Y., Liu, G. J., Yang, L., *et al*., 2018. Numerical modelling of elastic modulus and diffusion coefficient of concrete as a three-phase composite material. *Construction and Building Materials*, **189**: 1251-1263, https://doi.org/10.1016/j.conbuildmat.2018.08.191.

Liu, B., Zhou, J. K., Wen, X. Y., Guo, J. H., Zhang, X. Y., Deng, Z. H., *et al*., 2019. Experimental investigation on the impact resistance of carbon fibers reinforced coral concrete. *Materials*, **12**: 4000, DOI: 10.3390/ma12234000.

Lyu, B. C., Wang, A. G., Zhang, Z. H., Liu, K. W., Xu, H. Y., Shi, L., *et al*., 2019. Coral aggregate concrete: Numerical description of physical, chemical and morphological properties of coral aggregate. *Cement and Concrete Composites*, **100**: 25-34, https://doi.org/10.1016/j.cemconcomp.2019.03.016.

Ma, L. J., Li, Z., Liu, J. G., Duan, L. Q., and Wu, J. W., 2019. Mechanical properties of coral concrete subjected to uniaxial dynamic compression. *Construction and Building Materials*, **199**: 244-255, https://doi.org/10.1016/j.conbuildmat.2018.12.032.

Ma, L. J., Wu, J. W., Wang, M. Y., Dong, L., and Wei, H. Z., 2020. Dynamic compressive properties of dry and saturated coral rocks at high strain rates. *Engineering Geology*, **272**: 105615, https://doi.org/10.1016/j.enggeo.2020.105615.

Maage, M., Helland, S., Poulsen, E., Vennesland, Ø., and Carlsen, J., 1996. Service life prediction of existing concrete structures exposed to marine environment. *ACI Materials Journal*, **93**: 602-608, DOI: 10.14359/9866.

Meijers, S. J. H., Bijen, J. M. J. M., Borst, R. D., and Fraaij, A. L. A., 2005. Computational results of a model for chloride ingress in concrete including convection, drying-wetting cycles and carbonation. *Materials and Structures*, **38**: 145-154, https://doi.org/10.1007/BF02479339.

Real, S., and Bogas, J. A., 2018, Chloride ingress into structural lightweight aggregate concrete in real marine environment. *Marine Structures*, **61**: 170-187, https://doi.org/10.1016/j.marstruc.2018.05.008.

Tang, L. P., 2008. Engineering expression of the ClinConc model for prediction of free and total chloride ingress in submerged marine concrete. *Cement and Concrete Research*, **38**: 1092-1097, https://doi.org/10.1016/j.cemconres.2008.03.008.

Thomas, M. D. A., and Bamforth, P. B., 1999. Modelling chloride diffusion in concrete effect of fly ash and slag. *Cement and Concrete Research*, **29**: 487-495, https://doi.org/10.1016/S0008-8846(98)00192-6.

Wang, L., Song, Z. P., Yi, J., Li, J. Y., Fu, F., and Qian, K., 2019. Experimental studies on bond performance of BFRP bars reinforced coral aggregate concrete. *International Journal of Concrete Structures and Materials*, **13**: 52, https://doi.org/10.1186/s40069-019-0367-7.

Wang, Y., Zhang, S. H., Niu, D. T., Su, L., and Luo, D. M., 2020. Strength and chloride ion distribution brought by aggregate of basalt fiber reinforced coral aggregate concrete. *Construction and Building Materials*, **234**: 117390, https://doi.org/10.1016/j.conbuildmat.2019.117390.

Wu, Z. Y., Zhang, J. H., Yu, H. F., Ma, H. Y., Chen, L., Dong, W., *et al*., 2020. Coupling effect of strain rate and specimen size on the compressive properties of coral aggregate concrete: A 3D mesoscopic study. *Composites Part B: Engineering*, **200**: 108299, https://doi.org/10.1016/j.compositesb.2020.108299.

Yang, S. T., Yang, C., Huang, M. L., Liu, Y., Jiang, J. T., and Fan, G. X., 2018. Study on bond performance between FRP bars and seawater coral aggregate concrete. *Construction and Building Materials*, **173**: 272-288, https://doi.org/10.1016/j.conbuildmat.2018.04.015.

Yu, H. F., Da, B., Ma, H. Y., Zhu, H. W., Yu, Q., Ye, H. M., *et al*., 2017. Durability of concrete structures in tropical atoll environment. *Ocean Engineering*, **135**: 1-7, https://doi.org/10.1016/j.oceaneng.2017.02.020.

Yu, H. F., Sun, W., Yan, L. H., and Ma, H. Y., 2002. Study on prediction of concrete service life I – Theoretical model. *Journal of the Chinese Ceramic Society*, **30**: 686-690, DOI: 0454-5648(2002)06-0686-05 (in Chinese with English abstract).

Yu, H. F., Tan, Y. S., and Feng, T. T., 2019. Study of temporal change in chloride diffusion coefficient of concrete. *ACI Materials Journal*, **116**: 103-112, DOI: 10.14359/51710966.

Zhang, Y. S., Liu, C., Liu, Z. Y., Liu, G. J., and Yang, L., 2017. Modelling of diffusion behavior of ions in low-density and high-density calcium silicate hydrate. *Construction and Building Materials*, **155**: 965-980, https://doi.org/10.1016/j.conbuildmat.2017.08.128.

Zhang, Y. S., Sun, W., Chen, S. D., and Guo, F., 2011. Two- and three-dimensional chloride ingress into fly ash concrete. *Journal of Wuhan University of Technology – Materials Science Edition*, **26**: 978-982, https://doi.org/10.1007/s11595-011-0348-4.

(Edited by Ji Dechun)